Interdecadal Variability of Southeastern South America Rainfall and Moisture Sources during the Austral Summertime

VERÓNICA MARTÍN-GÓMEZ

Instituto de Física, Facultad de Ciencias, Universidad de la República, Montevideo, Uruguay

EMILIO HERNÁNDEZ-GARCIA

Instituto de Física Interdisciplinar y Sistemas Complejos, Campus Universitat de les Illes Balears, Palma de Mallorca, Spain

MARCELO BARREIRO

Instituto de Física, Facultad de Ciencias, Universidad de la República, Montevideo, Uruguay

CRISTÓBAL LÓPEZ

Instituto de Física Interdisciplinar y Sistemas Complejos, Campus Universitat de les Illes Balears, Palma de Mallorca, Spain

(Manuscript received 30 October 2015, in final form 13 June 2016)

ABSTRACT

Sea surface temperature (SST) anomalies over the tropical oceans are able to generate extratropical atmospheric circulation anomalies that can induce rainfall variability and changes in the sources of moisture. The work reported here evaluates the interdecadal changes in the moisture sources for southeastern South America (SESA) during austral summer, and it is divided into two complementary parts. In the first part the authors construct a climate network to detect synchronization periods among the tropical oceans and the precipitation over SESA. Afterward, taking into account these results, the authors select two periods with different degrees of synchronization to compare the spatial distribution of the SESA moisture sources.

Results show that during the last century there were three synchronization periods among the tropical oceans and the precipitation over SESA (during the 1930s, 1970s, and 1990s) and suggest that the main moisture sources of SESA are the recycling over the region, the central-eastern shore of Brazil together with the surrounding Atlantic Ocean, and the southwestern South Atlantic surrounding the SESA domain. Comparison of SESA moisture sources for the 1980s (a period of nonsignificant synchronization) and the 1990s (a synchronized period) shows that the principal differences are in the intensity of the recycling and in the strength of the central-eastern shore of Brazil. Moreover, the authors find that a region centered at (20°S, 300°E) is a moisture source for SESA only during the 1990s. These differences can be associated with the development of a low-level anticyclonic (cyclonic) anomaly circulation over central-eastern Brazil that favors the transport of moisture from central Brazil (central-eastern shore of Brazil) toward SESA in the 1990s (1980s).

1. Introduction

This study focuses on southeastern South America (SESA), a region that covers Uruguay and portions of northeastern Argentina and southern Brazil (see Table 1 and Fig. 1). SESA corresponds mostly to the southern part (south of 25°S) of the La Plata basin (LPB), the second largest basin in South America, which comprises parts of Brazil, Paraguay, Uruguay, Argentina, and Bolivia. SESA, located to the south of the Amazon basin, is one of the most densely populated regions in South America. Precipitation along with its variability is very important because it plays a key role in the generation of hydroelectric energy and in the economy, which over LPB is mainly based on harvesting and ranching (Berbery

Corresponding author address: V. Martín-Gómez, Instituto de Física, Universidad de la República de Uruguay, Iguá 4225, Montevideo 11400, Uruguay.
E-mail: vero.martin.gomez@gmail.com

DOI: 10.1175/JCLI-D-15-0803.1

TABLE 1. Geographical regions of each index that make up our network's nodes. The indices are defined considering the spectral average of the sea surface temperature (for TNA, Niño-3.4, TSA, ATL3, and IOD) and precipitation (for PCP) anomalies in the specified regions. In the Indian Ocean dipole case, the index is computed from the difference between the 2D average SST in the west region and the 2D average in the east region. Land areas are only considered for the case of the precipitation index.

		Earth's regions	
Index abbreviation	Index	Latitude range	Longitude range
Niño-3.4	Niño-3.4 (Trenberth 1997)	5°N–5°S	170°–120°W
TNA	Tropical North Atlantic	10°–30°N	60°–30°W
TSA	Tropical South Atlantic	5°–25°S	330°–358°E
ATL3	Equatorial Atlantic (Zebiak 1993)	3°N–3°S	0°–20°W
IOD	Indian Ocean dipole (Saji et al. 1999)	10°S–10°N	50°–70°E
		10°S–0°N	90°–110°E
PCP	Southeastern South America (SESA) precipitation (only land areas are considered)	25°–40°S	60°–50°W

and Barros 2002). Moisture that could lead to future precipitation over the region can come from two different sources: (i) water vapor advection from other regions and (ii) local recycling. While the advection of water vapor depends on the atmospheric circulation and can have two different origins (continental or oceanic), the recycling is the process by which evapotranspiration from a particular continental region returns as precipitation to the same region (Brubaker et al. 1993).

Previous moisture studies have focused mainly on the whole LPB and are described below for reference. One of the goals of this study is then to assess how much of the previous results found for the whole LPB apply to SESA. According to Martinez and Dominguez (2014), approximately 63% of the mean precipitation over LPB comes from South America and the remaining 37% comes mostly from the South Pacific and Atlantic Oceans. Studies have also shown that the main continental moisture source of the LPB is the Amazon basin (e.g., Martinez and Dominguez 2014; Zemp et al. 2014; Drumond et al. 2014; Dirmeyer et al. 2009; Berbery and Barros 2002), contributing 24% of the annual mean precipitation over the LPB (Martinez and Dominguez 2014). Using the concept of cascading moisture

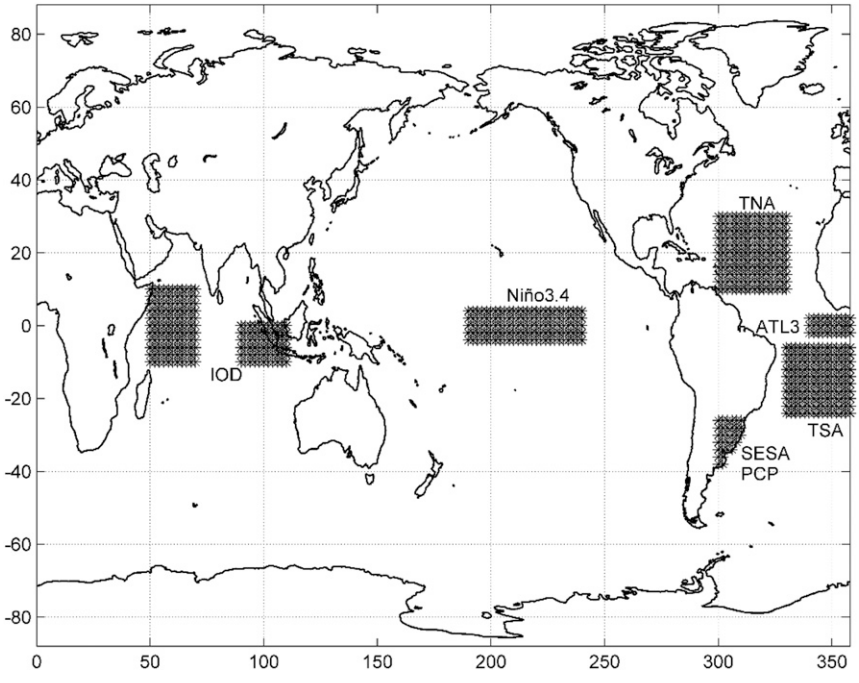

FIG. 1. Regions that represent the spatial domain over which the SST anomalies (over the oceans) and PCP anomalies (over the continent) are averaged to define the climate indices (or network's nodes).

recycling, which represents the moisture transport between two locations on the continent that evolves one or more reevaporation cycles along the way, Zemp et al. (2014) showed that the southern Amazon could act not only as the main direct continental moisture source of the LPB but also as an intermediate region that distributes moisture originating from the entire Amazon basin during the wet season (December to March). The transport of the southern Amazonian moisture toward the LPB takes place throughout the year, being a quasi-permanent source with a maximum during the austral summer season (Berbery and Barros 2002; Martinez and Dominguez 2014). The transport is carried out via the South American low-level jet (SALLJ) along the Andes (Marengo 2005; Martinez and Dominguez 2014).

Another continental type of moisture source but without advection from other regions is the local recycling. For the LPB, it represents 23.5% of its total annual mean precipitation and reaches its maximum during the austral summer season as a result of the enhancement of the large-scale convergence and net radiation, which increases the atmospheric instability, precipitation, and evaporation (Martinez and Dominguez 2014).

The Atlantic and Pacific Oceans are the main oceanic moisture sources of the LPB and are seasonally dependent (Drumond et al. 2008; Martinez and Dominguez 2014). Drumond et al. 2008 used a Lagrangian particle dispersion model to compute the trajectories of the particles in the atmosphere backward in time. They focused mainly on SESA and found that its main oceanic moisture sources are the southwestern South Atlantic, the tropical North Atlantic, and the surrounding Atlantic Ocean located near eastern-central Brazil. While the latter two remain as moisture sources throughout the year, the moisture from the tropical North Atlantic only reaches the LPB during the austral summer season. This is associated with the development of a cross-equatorial flow carrying moisture from the North Atlantic that penetrates into South America. Over the continent, the presence of the Andes forces the flow to become northerly and is channeled southward reaching the LPB (Drumond et al. 2008; Martinez and Dominguez 2014; Silva et al. 2012).

Regarding the Pacific Ocean, Martinez and Dominguez (2014) showed that the subtropical and extratropical part of the South Pacific contributes to LPB precipitation with 7.1% of the total annual mean precipitation, with its contribution being more important during the austral winter.

It is well known that the atmospheric circulation is sensitive to the ocean surface conditions in the tropics. Anomalies in the sea surface temperature (SST) over the tropical oceans are able to induce changes in the meridional circulation and generate stationary Rossby waves that propagate toward extratropical latitudes, processes that induce variations in the regional circulation patterns associated with rainfall.

For the particular case of SESA, several previous studies have shown that the SST anomalies in the tropical Pacific, Atlantic, and Indian Oceans can influence precipitation variability through atmospheric teleconnections (e.g., Seager et al. 2010; Barreiro et al. 2014; Grimm et al. 2000; Silvestri 2004; Barreiro and Tippmann 2008; Barreiro 2010; Diaz et al. 1998; Chan et al. 2008) as well as the moisture transport (e.g., Silva et al. 2009; Vera et al. 2004; Martinez and Dominguez 2014; Castillo et al. 2014).

El Niño–Southern Oscillation (ENSO) is one of the interannual variability phenomena that has been shown to influence the moisture transport from the Amazon basin toward LPB through changes in the intensity of the SALLJ (Silva et al. 2009; Vera et al. 2004; Martinez and Dominguez 2014). The physical mechanism through which the positive phase of El Niño induces an increase of the moisture of Amazonian origin in the LPB involves a weakening of the Walker circulation that increases anomalous subsidence over Brazil, which subsequently enhances upward motion over southeastern South America (Andreoli and Kayano 2005). This weakening in the local Hadley circulation between tropical and subtropical South America turns into a strengthening of the southward transport of moisture in lower levels from Brazil toward SESA, which is related to a larger number of SALLJ intensification events during the positive phase of ENSO (Silva et al. 2009).

Moreover, the warm phase of this equatorial Pacific phenomenon has been shown to increase the moisture from the South Pacific in the LPB (Martinez and Dominguez 2014). Martinez and Dominguez (2014) suggest that this could be due to the anomalous upper-level circulation pattern during the Niño events, where stronger subtropical westerlies occur together with an anomalous cyclone located over the South Pacific along with an anomalous anticyclone over the South Atlantic (Andreoli and Kayano 2005; Vera et al. 2004; Ropelewski and Halpert 1987).

Finally, the tropical oceans can interact with each other inducing SST anomalies in remote basins through atmospheric and oceanic teleconnections (e.g., Alexander et al. 2002; Enfield and Mayer 1997; Saravanan and Chang 2000; Rodriguez-Fonseca et al. 2009; Meyers et al. 2007; Wang and Wang 2014; Wu and Kirtman 2004; Yoo et al. 2013). All aforementioned studies focus on the impact that one particular ocean basin (or combination of two) can have on rainfall over SESA or on another basin. Recently Martín-Gómez and Barreiro (2016) used a methodology borrowed from complex networks to study how SST anomalies in the three tropical oceans can work

together to induce springtime rainfall variability over SESA. Martín-Gómez and Barreiro (2016) constructed a climate network considering Niño-3.4, the tropical North Atlantic (TNA), the Indian Ocean dipole (IOD), and SESA precipitation (SESA PCP) as the networks' nodes and focused on the detection of synchronization periods, understanding synchronization as those periods in the twentieth century in which there was significant interaction among several (or in the best case all) of the networks' components. Martín-Gómez and Barreiro (2016) were able to detect two different synchronization periods with a distinct combination of tropical oceans inducing SESA PCP anomalies. Martín-Gómez and Barreiro (2016) also described the possible physical mechanism through which SST anomalies in the tropical oceans could generate changes in the regional circulation over SESA and therefore induce rainfall anomalies. Thus, the relevance of studying the synchronization periods resides in the fact that, if SESA PCP is an interactive node, the tropical oceans induce SESA PCP variability and enhance its predictability. Moreover, different periods with different degrees of synchronization (e.g., a synchronized period vs a nonsignificant synchronized period) could have different associated atmospheric circulation patterns that induce changes in the moisture sources. Here we extend the study focusing on the summer season and find that there is a strong decadal variability in the impact of the oceans on SESA rainfall accompanied by large changes in moisture sources.

This study comprises two parts: In the first part, following the methodology of Tsonis et al. (2007) and Martín-Gómez and Barreiro (2016), we construct a climate network in order to detect different synchronization periods among the tropical oceans and precipitation over SESA. In the second part we select two periods with different degrees of synchronization, and, employing a Lagrangian particle dispersion model, we calculate and compare the trajectories of the atmospheric moisture in both cases. This provides information about the spatial distribution of the moisture sources of SESA and allows the analysis of their changes.

2. Construction of the climate network and synchronization measure

A climate network is constructed considering the following five different tropical oceanic indices as network nodes (see Fig. 1 and Table 1): Niño-3.4, the TNA, the tropical South Atlantic (TSA), the equatorial Atlantic (ATL3), and the IOD, as well as a precipitation index over SESA. The election of the indices takes into account all the tropical basins that are known to influence SESA precipitation during the austral summertime. The oceanic indices are defined considering the monthly mean SST from the Extended Reconstructed SST, version 3 (ERSSTv3b; Smith et al. 2008; Xue et al. 2003), with a resolution of $2° \times 2°$. The precipitation index is defined using the monthly mean observed data from the Global Precipitation Climatology Centre, version 5 (GPCCv5; Schneider et al. 2011) dataset, with a resolution of $1° \times 1°$. The period of study is 1901–2005.

We also consider the monthly mean values of the vertical integral of the horizontal divergence of the moisture flux from ECMWF interim reanalysis (ERA-Interim) data as well as monthly means of the winds at 850 hPa and monthly means of the geopotential height at 200 hPa obtained from the ECMWF data server (Dee et al. 2011). These fields are used to diagnose circulation anomalies and understand the changes in the moisture sources for SESA in different periods. The available data span the period 1979 to present, so to compute the anomaly values of all the products from ERA-Interim employed in this work (vertical integral of the horizontal divergence of the moisture flux, winds at 850 hPa, and geopotential height at 200 hPa), we consider the climatological mean from the common period (1979–2005).

The methodology followed to construct the network is described in detail in Martín-Gómez and Barreiro (2016). Here we provide a summarized version. It consists of several steps:

1) The climate indices are defined by spatially averaging the SST or precipitation anomalies in the respective regions (Table 1) within individual trimesters: September–November (SON) for the case of the Niño-3.4 index and December–February (DJF) for the other indices (TNA, TSA, ATL3, IOD, and PCP). In this situation, each one of the time series values represents the seasonal mean of the monthly anomaly values of the SST (tropical oceanic regions) or PCP (SESA region, only land areas). The anomaly values of the indices were computed as the deviation from the monthly climatological mean during the period (1901–2005). Therefore, our time series have 105 values, one per year. Each time series will be a node in a climate network. The lag time of 3 months among Niño-3.4 and the rest of the nodes was established in order to allow them to respond to the atmospheric anomalies generated by the equatorial Pacific.
2) For each year, a climate network is constructed by computing the Spearman correlation coefficient ρ_{ij}^{t} among each pair i,j of time series in the interval $[t - (\Delta t/2), t + (\Delta t/2)]$. This correlation is a measure of the strength of the connection between the corresponding pair of nodes at the time t in the

middle of a sliding window of length $\Delta t = 11$ yr. The mean network distance is computed as a measure of synchronization among the nodes:

$$d(t) = \frac{2}{N(N-1)} \sum_{i<j} \sqrt{2(1 - |\rho_{ij}^t|)}, \quad (1)$$

where N is the number of network nodes (in this case, 6). Note that the network is completely synchronized when the distance is zero and uncorrelated nodes give a value of $\sqrt{2}$ to the distance.

3) To compute the statistical significance of the mean network distance we employ the Monte Carlo method under the following criterion: we consider a red noise null model for those nodes with autocorrelation coefficient at lag 1 significant at the 95% level in a one-tailed t test. In the opposite case we consider white noise. Following this criterion, only the TNA and TSA can be considered as red noise. Then, we generate 1000 surrogate time series of each index under these null hypotheses and compute the network distance time series considering a sliding window of 11-yr length. In this way, we construct 1000 surrogate time series of the mean network distance, which allows determining the 5% significance level. We consider that there is a statistically significant synchronization event when the mean network distance is below this threshold for more than 7 consecutive years.
4) Finally, we also define the relative precipitation weight (RPW) in order to check the importance of PCP as a network's node, understanding "importance" as the degree of interaction of the precipitation index with the rest of the nodes. The definition of RPW(t) is given by

$$\mathrm{RPW}(t) = \frac{\frac{\sqrt{2}}{3} - d_{\mathrm{PCP}}(t)}{\sqrt{2} - d(t)}, \quad (2)$$

where d_{PCP} is proportional to the mean network distance from PCP to the tropical oceanic indices in Eq. (1):

$$d_{\mathrm{PCP}}(t) = \frac{2}{N(N-1)} \sum_{i \neq \mathrm{PCP}} \sqrt{2(1 - |\rho_{i,\mathrm{PCP}}^t|)}, \quad (3)$$

where $N = 6$ (the number of network nodes) and $\rho_{i,\mathrm{PCP}}^t$ is the Spearman correlation coefficient between PCP and the oceanic index i. The maximum and minimum values of the RPW are one and zero, in such a way that higher values of the RPW are associated with a larger influence of the tropical oceans on rainfall and vice versa. RPW = 1 takes place when $d_{\mathrm{PCP}} = 0$ (correlation coefficient between each one of the oceanic indices and PCP index are 1 or −1), and the tropical oceans are completely disconnected among them. RPW = 0 means that SESA precipitation is completely disconnected from the oceanic indices. See more details in Martín-Gómez and Barreiro (2016).

3. Lagrangian model and identification of moisture sources

To get information about the spatial distribution of the moisture sources of SESA, we consider a Lagrangian flexible particle dispersion model (FLEXPART; Stohl et al. 2005) driven by the 6-h forecast from the Climate Forecast System Reanalysis (CFSR; Saha et al. 2010) with a resolution of 0.5° × 0.5° during the period 1979 to 2000. We consider the CFSR data because this reanalysis is able to reproduce correctly the lower- and upper-level atmospheric circulation patterns and precipitation distribution over South America during the austral summer season (Silva et al. 2012; Quadro et al. 2013).

FLEXPART is a Lagrangian particle dispersion model able to calculate and track the trajectories of the atmospheric moisture running forward and backward in time while dividing the atmosphere into a large number of particles (Stohl et al. 2005). Each particle represents a mass of air with a given mass m that is transported by the 3D wind field, which includes modeled turbulence. In our work, the vertical distribution of the particles in the atmosphere is proportional to the air density, and the moisture sources are computed through the net budget of evaporation minus precipitation obtained from the changes in the moisture along the particles' trajectories. As in Stohl and James (2004, 2005) and in Drumond et al. (2008), the steps are as follows:

1) We select the vertical atmospheric column located over SESA (see spatial domain on Table 1), from where we release 50 000 particles per simulation with a vertical distribution proportional to the air density. We perform five simulations per month (December–January–February) releasing the particles on the 12th, 16th, 20th, 24th, and 28th of each month. All these particles are transported by FLEXPART backward in time for 10 days and tracked recording their positions and specific humidity every 6 h. We limit the transport of the particles to 10 days because it represents the average time that the water vapor resides in the atmosphere (Numaguti 1999). In turn, we establish a lag time between consecutive simulations of 4 days in order to

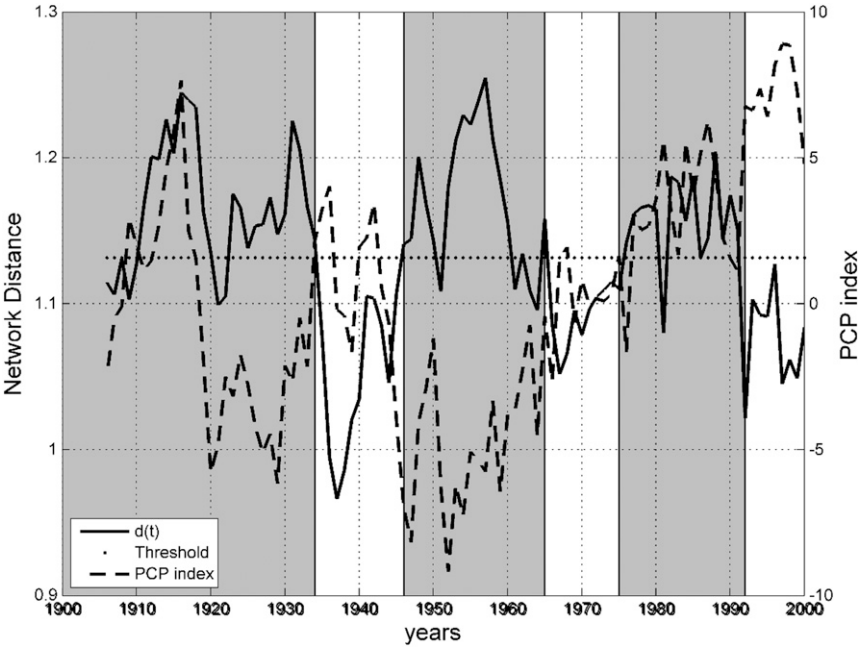

FIG. 2. Mean network distance time series during the twentieth century computed from Eq. (1) (solid black curve). To compute this time series, Niño-3.4 is centered on SON; TNA, TSA, ATL3, IOD, and PCP are centered on DJF. The dashed black line represents the precipitation index over SESA in austral summer (DJF), and the horizontal black dotted line represents the 5% significance level below which the distance identifies significant synchronization. Each point of the network distance time series represents the value of the mean network distance computed considering a sliding window of 11-yr length $[t-(\Delta t/2), t+(\Delta t/2)]$ centered on year t. The gray (white) bands indicate the nonsynchronization (synchronized) periods.

ensure that the obtained particle trajectories are different in consecutives simulations since the lifetime of the synoptic perturbation is around 5 days. We have checked in specific date ranges that performing daily releases instead of the selected five releases per month does not alter our results.

2) The net budget evaporation e minus precipitation p of each particle i with mass m was computed through changes in the specific humidity q along its trajectory:

$$(e-p)_i = \left(m\frac{dq}{d\tau}\right)_i. \tag{4}$$

The $(e-p)_i$ parameter was calculated for specific days. We called $(e-p)_{i,n}$ the net budget evaporation minus precipitation of the particle i during the nth day of trajectory. Remember that we release the particles the 10th day of trajectory and run the model back in time, so for example $(e-p)_{i,1}$ will represent the net budget evaporation minus precipitation of the particle i during the first day of trajectory, which is developed from day 10 to the day 9. In general terms, this can be mathematically expressed as follows:

$$(e-p)_{i,n} = \left[m_i\frac{q_{i,\text{day}=(10-n+1)} - q_{i,\text{day}=(10-n)}}{\Delta\tau}\right], \tag{5}$$

where $\Delta\tau = 1$ day.

3) We define a $1^\circ \times 1^\circ$ grid and per each day of trajectory, we add $(e-p)_{i,n}$ for all the particles i of the vertical column located over an area A, obtaining the net budget $(E-P)_n$ where E and P are evaporation and precipitation rates for the whole vertical column of area A in each grid point and during the nth day of trajectory:

$$(E-P)_n = \frac{\sum_{i;\text{vertical\_column}} (e-p)_{i,n}}{\sigma \text{Area}_{\text{column}}}, \tag{6}$$

where σ represents the density of the water. The expression in (6) gives the net budget as equivalent height of water per unit of time.

4) Finally, we take the average of the 10 net budgets $(E-P)_n$, and call it $(E-P)^{10}$. Per each grid cell, the parameter $(E-P)^{10}$ will represent the net budget evaporation minus precipitation in the whole vertical column located over an area A (the area of the grid cell) averaged over the 10 days of trajectory of the

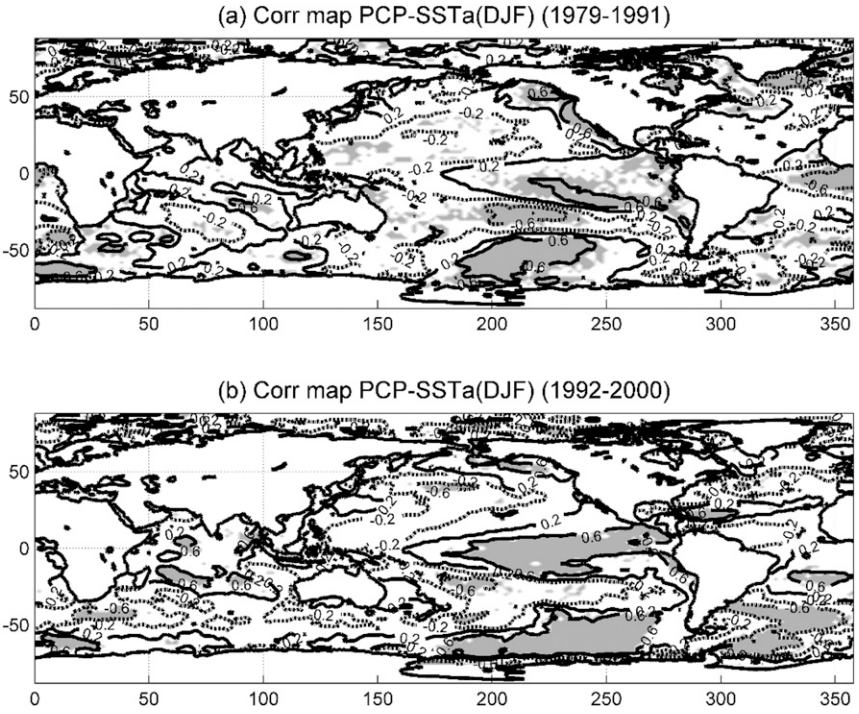

FIG. 3. Spearman correlation maps between the PCP index over SESA and the SST anomalies centered on the austral summer season (DJF) for the (a) 1980s and (b) 1990s. The anomaly values were computed considering the deviation from the climatological period (1901–2005). The gray domains represent those regions that are statistically significant at the 95% significance level in a Monte Carlo test based on the generation of 100 surrogate time series.

particles going toward SESA [see Eq. (7)]. The positive (negative) values of $(E-P)^{10}$ will represent the regions where particles when passing gain (lose) moisture on average over the 10 days of trajectory toward SESA, and therefore these regions will represent sources (sinks) of moisture.

$$(E-P)^{10} = \frac{1}{10}\sum_{n=1}^{10}(E-P)_n. \qquad (7)$$

4. Climate network and synchronization periods

Figure 2 shows the network distance (solid black line) and the PCP index on DJF (dashed black line) during the last century. Regarding the mean network distance, the major features are the following:

1) The network distance is characterized by interannual and interdecadal variability.
2) During the last century there were three synchronization periods (distance smaller than the significance level): 1934–46, 1965–75, and 1992–2000, marked by white bands in Fig. 2.

The existence of synchronization periods indicates that several (or in the best case all) of the nodes in the network are interacting. However, this does not ensure that during these periods the oceans are influencing rainfall over SESA. To address this question we compute the Spearman correlation coefficient between the mean network distance and a precipitation index over SESA constructed taking averages of 11-yr sliding windows from SESA PCP index. The resulting correlation coefficient, −0.25, is statistically significant at the 5% significance level in a one-sided t test (threshold level is 0.17), suggesting that an increase of the network distance (a decrease in the synchronization among the network's nodes) is associated with less precipitation over SESA. The anticorrelation is evident in Fig. 2. However, this result does not completely ensure the increment of SESA precipitation as a consequence of enhancing the degree of synchronization of the network. To further address this issue we compute the Spearman correlation coefficient between the RPW and the mean network distance. The obtained value, −0.22, is statistically significant at the 5% significance level in a one-sided t test, suggesting that a larger connectivity of the precipitation index is associated with a smaller network

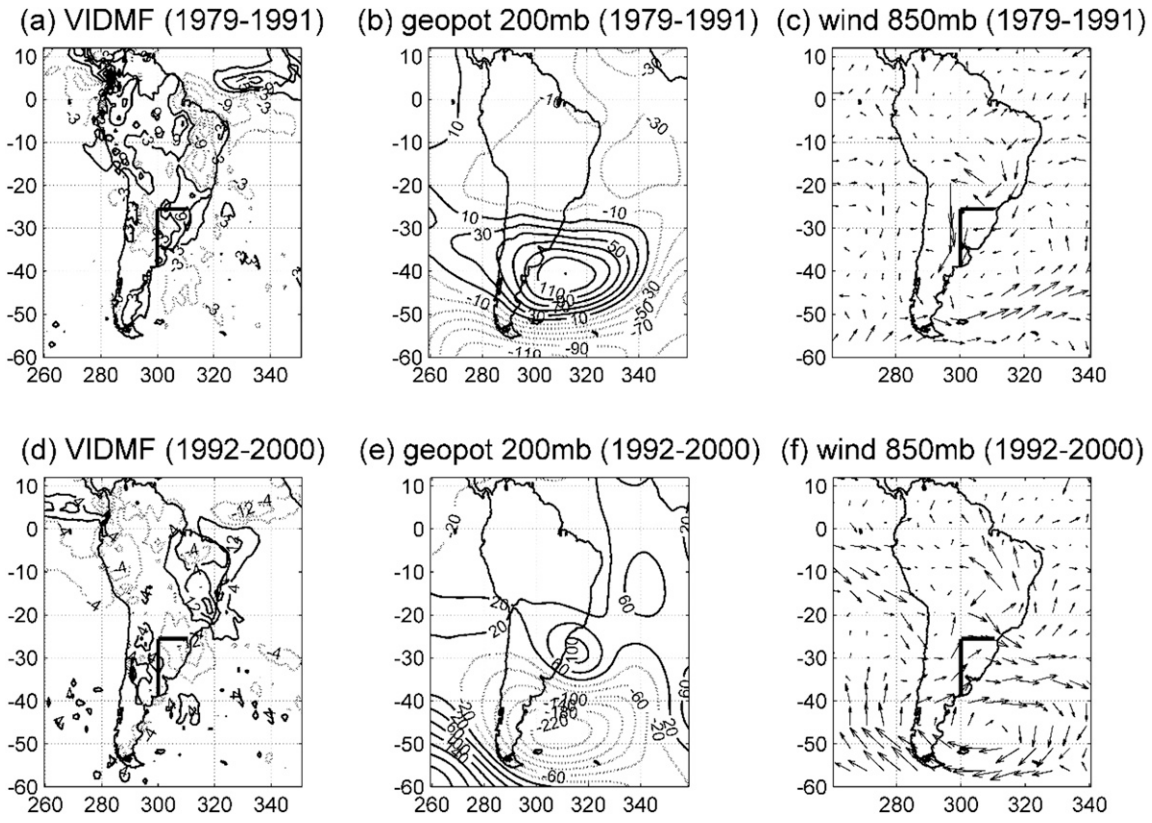

FIG. 4. Anomaly VIDMF in kg m^{-2} s^{-2} (the values are divided by the scale factor 10^{-6}) for (a) 1979–91 and (d) (1992–2000). Anomaly eddy geopotential height (geopot) at 200 mb in m^2 s^{-2} for (b) 1979–91 and (e) 1992–2000. Anomaly winds at 850 mb in m s^{-1} for (c) 1979–91 and (f) 1992–2000. The marked region over South America represents the domain where the PCP over SESA index was defined.

distance (larger synchronization of the network). On the other hand, we also computed the correlation coefficient between the RPW and the precipitation, obtaining the value 0.24, also statistically significant at the 5% significance level in a one-sided t test. These results suggest that an increment of the precipitation in SESA is related to a larger influence of the tropical oceans on SESA, which in turn is associated with a greater degree of synchronization.

Thus, one could conclude that more synchronization of the network is associated with an increase of the precipitation over SESA. Nevertheless, we note that there are periods in which precipitation is above normal, but the network does not show significant synchronization (e.g., during the decades of 1910s and 1980s).

5. Moisture sources of SESA during the 1980s and 1990s

Given the availability of ERA-Interim and CFSR data, we focus our discussion on the differences between the 1980s (1979–91) and 1990s (1992–2000), a period of nonsignificant synchronization and another of statistically significant synchronization among network components, respectively. Note that in Fig. 1 SESA PCP anomalies were computed as a departure from the climatological mean of the period 1901–2005, obtaining positive values in both the 1980s and 1990s. If we consider only the period 1979–2000, the 1980s have rainfall below the mean, while the 1990s have rainfall above the mean in SESA.

We first analyze SST and circulation anomalies in the two periods. The Spearman correlation map between the SESA precipitation index (in DJF) and the SST anomalies (in SON) for the two periods (1980s and 1990s) are shown in Fig. 3 (the Spearman correlation map between SST anomalies in SON and SESA PCP in DJF was also computed, but given that the same conclusions can be obtained by comparing SON and DJF figures, here we only show the DJF map). The shaded regions are statistically significant at the 5% significance level in a Monte Carlo test based on the generation of 100 surrogate time series. The first distinctive feature between these two decades is that while in the 1990s the equatorial Pacific dominates, during the 1980s the

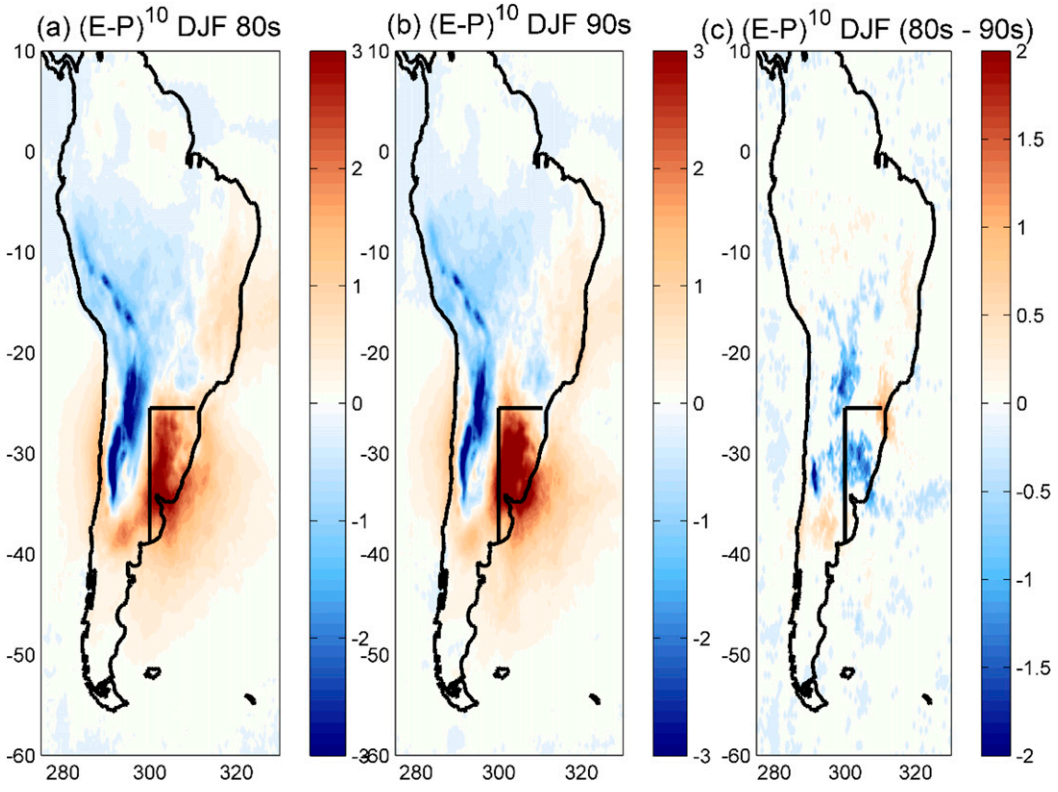

FIG. 5. (a) The 10-day average of the net budget evaporation minus precipitation $[(E - P)^{10}]$ during the 1980s (1979–91) in DJF; (b) as in (a), but for the 1990s (1992–2000). (c) Difference between the 1980s and 1990s. Only locations with a difference significant at the 90% confidence level considering a Monte Carlo approach are colored. The $(E - P)^{10}$ values were computed from a backward Lagrangian experiment considering SESA as the target area. Units: mm day^{-1}.

equatorial Atlantic shows stronger correlation. The net value of the areal vertical integral of moisture flux divergence, -2.66×10^{-4} kg m^{-2} s^{-2} (1.29×10^{-4} kg m^{-2} s^{-2}), is consistent with the increased (decreased) rainfall over SESA during the 1990s (1980s). See Figs. 4a,d, where the anomaly vertical integral divergence moisture flux (VIDMF) is shown. VIDMF was computed as follows: We first removed the climatological mean from 1979 to 2005 and applied the Lanczos filter to the time series. After that we computed the DJF average for each period to obtain the anomalies.

Figures 4b,e show the anomalous eddy geopotential height at 200 mb during 1980s and 1990s, respectively. They were computed by 1) removing the climatology of the period 1979–2005, 2) applying the low-pass Lanczos filter to the time series, and 3) removing the zonal average of the geopotential height at 200 mb. Finally, from these anomaly values we select the DJF season and construct the average over the periods 1979–91 and 1992–2000. Focusing on Fig. 4b, the 1980s are characterized by an anomalous anticyclone located southeast of South America over the Atlantic Ocean and an anomalous cyclone over southern South America. This situation does not favor the convergence of moisture over SESA and inhibits vertical ascent motions. However, during the 1990s the subtropical dipole of cyclonic–anticyclonic circulation anomalies in subtropical South America favors the advection of cyclonic vorticity and ascent motion over SESA and therefore the increase of the precipitation (Fig. 4e). The low-level wind anomalies are consistent with this picture, showing mainly divergence (convergence) over SESA during the 1980s (1990s) (see Figs. 4c,f). Figures 4c,f were computed following the same procedure indicated for Figs. 4a,d.

Figures 5a and 5b represent the 10-day average of the net budget evaporation minus precipitation $[(E - P)^{10}]$ over the periods 1979–91 and 1992–2000, respectively. Regions with positive (negative) values of this variable are associated with a net profit (loss) of moisture of the particles when passing by along their trajectories toward SESA, and, therefore, these regions will represent the main moisture sources (sinks) of SESA. From Figs. 5a,b we can see that the main moisture source

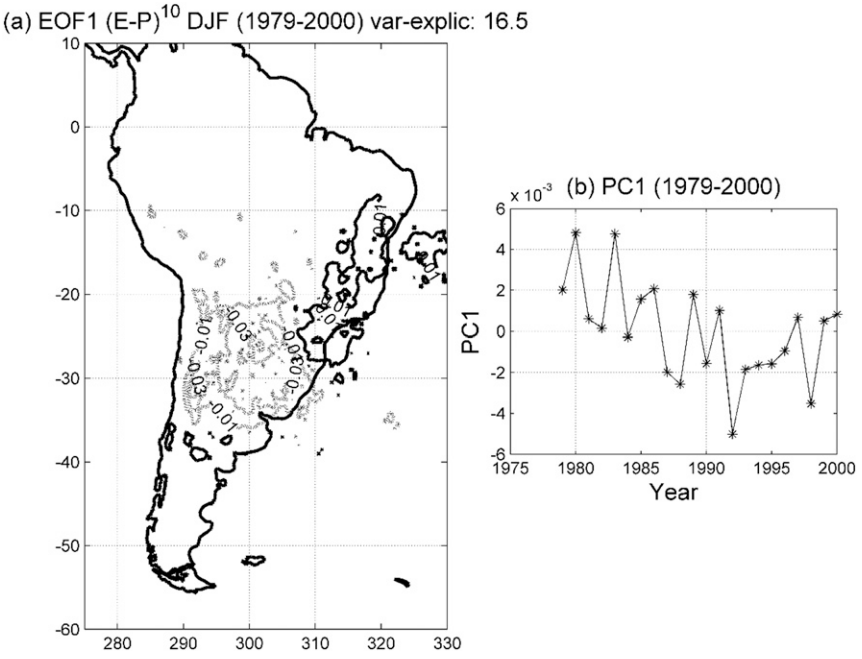

FIG. 6. (a) First EOF of $(E - P)^{10}$ and (b) its associated PC1. Period (1979–2000).

regions [with positive values of the $(E - P)^{10}$] are the recycling over SESA, the central-eastern shore of Brazil together with its surrounding Atlantic Ocean, and the South Atlantic Ocean surrounding the SESA shore. Results are almost in agreement with Fig. 1d from Drummond et al. (2008). The main difference arises over the central Brazil/Amazon basin, a region that in the previously mentioned study is characterized by positive values of the $(E - P)^{10}$ budget while in our case takes negative values. The difference is mainly associated with the reanalysis data employed to drive the FLEXPART model; while we consider the CFSR, Drumond et al. (2008) employed a reanalysis from ECMWF. Other factors that could introduce differences are that the selected domain for SESA is not exactly the same and that we consider December–February, while Drumond et al. (2008) consider the January–March season. However, when testing whether these can account for differences [computing the net budget $(E - P)^{10}$ under the same conditions as in Drumond et al. (2008)], results show an $(E - P)^{10}$ pattern with the same characteristics that we can observe in Fig. 5, suggesting that the target area and time period cannot explain differences and that the data considered is the main source of differences.

Figure 5c shows the differences in $(E - P)^{10}$ during the 1980s and 1990s that are significant at the 10% level. It suggests that during the 1980s the central-eastern shore of Brazil acted as a stronger moisture source, while during the 1990s the intensity of the recycling was larger. Moreover, during the 1990s the region at 60°W between 20° and 25°S acted as a moisture source, not clearly present during the 1980s. The stronger intensity of the recycling over SESA during the 1990s would be in agreement with the positive PCP anomalies observed in Fig. 2 and the anomalous vertical integral of the moisture convergence shown in Fig. 4d.

To interpret the changes in the moisture sources we compute the empirical orthogonal functions (EOFs) for the net budget $(E - P)^{10}$. Figure 6a shows the first EOF pattern that explains 16.5% of the $(E - P)^{10}$ variance. Its associated principal component (PC) is plotted in Fig. 6b. The EOF1 pattern shows a dipole-like structure with two centers of action, one located over central-eastern and southeastern Brazil and another one with opposite sign in the subtropical region located to the east of the Andes (20°–35°S, 295°–305°E). The associated PC1 shows a clear jump between both decades of study (1980s and 1990s; see Fig. 6b). Positive (negative) values of the PC1 tend to prevail before 1991 (after 1991), suggesting that the center located over central-eastern and southeastern Brazil would take positive (negative) values, and therefore, the particles that pass through that region along their trajectory toward SESA will load more (less) moisture. This center of action is associated with the statistically significant positive signal observed in Fig. 5c over central-eastern and southeast Brazil. The other center of action of the EOF1 pattern has the opposite sign and could be related to the two statistically significant negative signals observed in Fig. 5c over the subtropical region located to the east of the

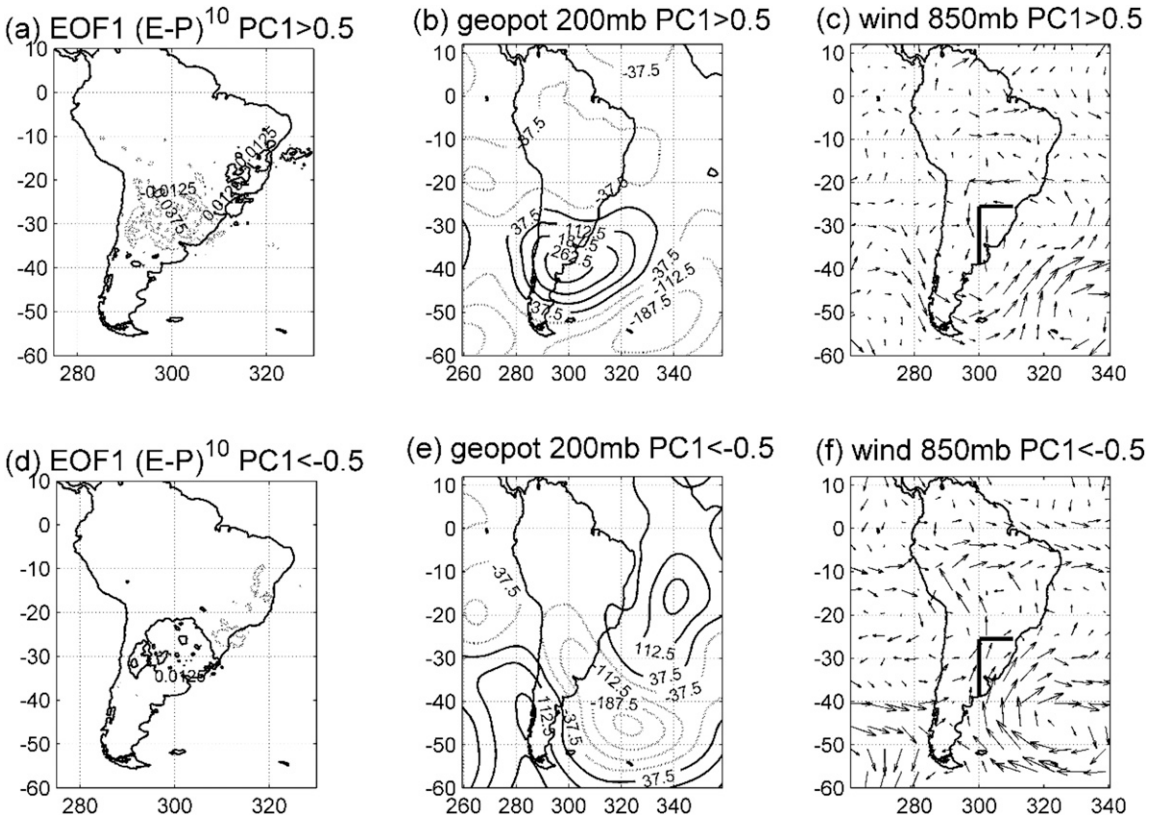

FIG. 7. Composite maps of the (a),(d) EOF1, (b),(e) eddy geopotential height at 200 mb, and (c),(f) low-level winds at 850 mb. Composites in (a),(b),(c) were constructed as the difference between extreme positive PC1 years (those with standardized PC1 > 0.5) and the neutral years. Composites in (d),(e),(f) were calculated as the difference between extreme negative PC1 years (those with standardized PC1 < -0.5) and the neutral.

Andes. Comparing Figs. 4c and 4f suggests that during the 1980s the northerly anomalies along the coast of central-eastern and southern Brazil associated with a cyclonic circulation at (15°S, 50°W) help the transport of moisture toward SESA. During the 1990s the situation is the opposite: a low-level anticyclonic circulation developed over central-eastern Brazil that does not favor the advection of moisture from the central-eastern shore of Brazil toward SESA, decreasing the contribution of this region as a moisture source. Instead, it favors the transport of moisture from the Amazon basin and can explain the extension of the region acting as moisture source toward the north of SESA in that decade. Note that the development of this low-level cyclonic (anticyclonic) anomaly circulation over central-eastern Brazil during the 1980s (1990s) is, in turn, consistent with the observed convergence anomaly of the vertical integral of moisture flux over the region shown in Fig. 4a (Fig. 4d).

Thus, during the 1990s there is an increase in cyclonic vorticity advection in upper levels and enhanced low-level convergence, resulting in a larger precipitation in SESA with respect to the 1980s.

We also perform the composite maps of the EOF1, the eddy geopotential height at 200 mb, and the low-level winds constructed as the difference between extreme-PC1 years [we take as extreme positive (negative) PC1 years those with standardized PC1 more (less) than 0.5 (-0.5)] and neutral years (see Fig. 7). Results show that the circulation patterns obtained from the composite analysis (both, positive, and negative extremes composite analysis) are similar to those shown on Figs. 4b,e. There are some differences between the patterns of Figs. 4 and 7, but the main spatial structures are easily distinguished, and, thus, EOF1 represents well the changes observed during both decades.

6. Conclusions

The atmosphere is sensitive to the ocean surface conditions in the tropics in such a way that SST

anomalies over the tropical oceans are able to generate quasi-stationary Rossby waves that propagate from the tropics toward extratropical latitudes inducing regional circulation anomalies that can induce not only rainfall variability but also changes in the sources of moisture. The work reported here has two complementary parts. In the first part we construct a climate network to detect synchronization periods among the tropical oceans and the precipitation over SESA during the austral summer season. Afterward, taking into account these results, we select two periods with different degrees of synchronization to compare the spatial distribution of the moisture sources. To do so we employ a Lagrangian particle dispersion model that allows the calculation and tracking of the trajectories of atmospheric moisture.

Results show that during the last century the network distance was characterized by interannual and interdecadal variability having three synchronization periods among the tropical oceans and the precipitation over SESA, which developed during the 1930s, 1970s, and 1990s. The relationship between the mean network distance and the precipitation over SESA is such that a larger degree of synchronization among the network's component (smaller mean network distance) is associated with an increase of the oceanic influence on SESA precipitation.

We then focus on the differences between the 1980s (1979–91) and the 1990s (1992–2000), one period of nonsynchronization and another of statistically significant synchronization among the tropical oceans and SESA precipitation. The comparison yielded the following conclusions:

1) When the synchronization of the network is statistically significant (1990s) there is convergence of moisture and favoring conditions for ascent motions over SESA, allowing an increase of the SESA precipitation. The opposite conditions can be observed in the period of nonsynchronization (1980s) resulting in reduced rainfall.
2) The main moisture sources of SESA are the recycling over the region, the central-eastern shore of Brazil together with its surrounding Atlantic Ocean, and the southwestern South Atlantic surrounding the SESA domain.
3) The main differences between the two selected decades are in the intensity of the recycling, in the intensity of the central-eastern shore of Brazil, and in a region centered at (20°S, 300°E). The latter is a moisture source for SESA only during the 1990s and is associated with the development of a low-level anticyclonic anomaly circulation over central-eastern Brazil that favors the transport of moisture from that region toward SESA. On the other hand, during the 1980s a low-level cyclonic anomaly circulation developed over central-eastern Brazil that favors a stronger advection of moisture from the central-eastern shore of Brazil.

Acknowledgments. The research leading to these results has received funding from the European Community's Seventh Framework Programme [FP7/2007-2011] under Grant Agreement 289447 (ITN LINC).
EHG and CL acknowledge support from FEDER and MINECO (Spain) through project ESCOLA (CTM2012-39025-C02-01).

REFERENCES

Alexander, M., A. I. Bladé, M. Newman, J. R. Lanzante, N. C. Lau, and J. D. Scott, 2002: The atmospheric bridge: The influence of ENSO teleconnections on air–sea interaction over the global oceans. *J. Climate*, **15**, 2205–2231, doi:10.1175/1520-0442(2002)015<2205:TABTIO>2.0.CO;2.

Andreoli, R. V., and M. T. Kayano, 2005: ENSO-related rainfall anomalies in South America and associated circulation features during warm and cold Pacific decadal oscillation regimes. *Int. J. Climatol.*, **25**, 2017–2030, doi:10.1002/joc.1222.

Barreiro, M., 2010: Influence of ENSO and South Atlantic Ocean on climate predictability over southeastern South America. *Climate Dyn.*, **35**, 1493–1508, doi:10.1007/s00382-009-0666-9.

——, and A. Tippmann, 2008: Atlantic modulation of El Niño influence on summertime rainfall over southeastern South America. *Geophys. Res. Lett.*, **35**, L16704, doi:10.1029/2008GL035019.

——, N. Diaz, and M. Remon, 2014: Role of the oceans and land–atmosphere interaction on summertime interdecadal variability over northern Argentina. *Climate Dyn.*, **42**, 1733–1753, doi:10.1007/s00382-014-2088-6.

Berbery, E. H., and V. R. Barros, 2002: The hydrologic cycle of the La Plata basin in South America. *J. Hydrometeor.*, **3**, 630–645, doi:10.1175/1525-7541(2002)003<0630:THCOTL>2.0.CO;2.

Brubaker, K. L., D. Entekhabi, and P. S. Eagleson, 1993: Estimation of continental precipitation recycling. *J. Climate*, **6**, 1077–1089, doi:10.1175/1520-0442(1993)006<1077:EOCPR>2.0.CO;2.

Castillo, R., R. Nieto, A. Drumond, and L. Gimeno, 2014: The role of the ENSO cycle in the modulation of moisture transport from major oceanic moisture sources. *Water Resour. Res.*, **50**, 1046–1058, doi:10.1002/2013WR013900.

Chan, S. C., S. K. Behera, and T. Yamagata, 2008: Indian Ocean dipole influence on South American rainfall. *Geophys. Res. Lett.*, **35**, L14S12, doi:10.1029/2008GL034204.

Dee, D. P., and Coauthors, 2011: The ERA-Interim reanalysis: Configuration and performance of the data assimilation system. *Quart. J. Roy. Meteor. Soc.*, **137**, 553–597, doi:10.1002/qj.828.

Diaz, A. F., C. D. Studzinski, and C. R. Mechoso, 1998: Relationships between precipitation anomalies in Uruguay and southern Brazil and sea surface temperature in the Pacific and Atlantic Oceans. *J. Climate*, **11**, 251–271, doi:10.1175/1520-0442(1998)011<0251:RBPAIU>2.0.CO;2.

Dirmeyer, P. A., K. L. Brubaker, and T. DelSole, 2009: Import and export of atmospheric water vapor between nations. *J. Hydrol.*, **365**, 11–22, doi:10.1016/j.jhydrol.2008.11.016.

Drumond, A., R. Nieto, L. Gimeno, and T. Ambrizzi, 2008: A Lagrangian identification of major sources of moisture over central Brazil and La Plata basin. *J. Geophys. Res.*, **113**, D14128, doi:10.1029/2007JD009547.

——, J. Marengo, T. Ambrizzi, R. Nieto, L. Moreira, and L. Gimeno, 2014: The role of the Amazon basin moisture in the atmospheric branch of the hydrological cycle: A Lagrangian analysis. *Hydrol. Earth Syst. Sci.*, **18**, 2577–2598, doi:10.5194/hess-18-2577-2014.

Enfield, D. B., and D. A. Mayer, 1997: Tropical Atlantic sea surface temperature variability and its relation to El Niño-Southern Oscillation. *J. Geophys. Res.*, **102**, 929–945, doi:10.1029/96JC03296.

Grimm, A. M., V. R. Barros, and M. E. Doyle, 2000: Climate variability in southern South America associated with El Niño and La Niña events. *J. Climate*, **13**, 35–58, doi:10.1175/1520-0442(2000)013<0035:CVISSA>2.0.CO;2.

Marengo, J. A., 2005: Characteristics and spatio-temporal variability of the Amazon River basin water budget. *Climate Dyn.*, **24**, 11–22, doi:10.1007/s00382-004-0461-6.

Martinez, J. A., and F. Dominguez, 2014: Sources of atmospheric moisture for the La Plata River basin. *J. Climate*, **27**, 6737–6753, doi:10.1175/JCLI-D-14-00022.1.

Martín-Gómez, V., and M. Barreiro, 2016: Analysis of ocean's influence on spring time rainfall variability over southeastern South America during the 20th century. *Int. J. Climatol.*, **36**, 1344–1358, doi:10.1002/joc.4428.

Meyers, G., P. Mcintosh, L. Pigot, and M. Pook, 2007: The years of El Niño, La Niña, and interactions with the tropical Indian Ocean. *J. Climate*, **20**, 2872–2880, doi:10.1175/JCLI4152.1.

Numaguti, A., 1999: Origin and recycling processes of precipitating water over the Eurasian continent: Experiments using an atmospheric general circulation model. *J. Geophys. Res.*, **104**, 1957–1972, doi:10.1029/1998JD200026.

Quadro, M. F., E. H. Berbery, M. S. Dias, D. L. Herdies, and L. G. Gonçalves, 2013: The atmospheric water cycle over South America as seen in the new generation of global reanalyses. *AIP Conf. Proc.*, Berlin, Germany, American Institute of Physics, 732–735, doi:10.1063/1.4804874.

Rodriguez-Fonseca, B., I. Polo, J. Garcia-Serrano, T. Losada, E. Mohino, C. R. Mechoso, and F. Kucharski, 2009: Are Atlantic Niño enhancing Pacific ENSO events in recent decades? *Geophys. Res. Lett.*, **36**, L20705, doi:10.1029/2009GL040048.

Ropelewski, C. F., and M. S. Halpert, 1987: Global and regional scale precipitation patterns associated with the El Niño/Southern Oscillation. *Mon. Wea. Rev.*, **115**, 1606–1626, doi:10.1175/1520-0493(1987)115<1606:GARSPP>2.0.CO;2.

Saha, S., and Coauthors, 2010: NCEP Climate Forecast System Reanalysis (CFSR) 6-hourly products, January 1979 to December 2010. Computational and Information Systems Laboratory, National Center for Atmospheric Research, doi:10.5065/D69K487J.

Saji, N. H., B. N. Goswami, P. N. Vinayachandran, and T. Yamagata, 1999: A dipole mode in the tropical Indian Ocean. *Nature*, **401**, 360–363.

Saravanan, R., and P. Chang, 2000: Interaction between tropical Atlantic variability and El Niño–Southern Oscillation. *J. Climate*, **13**, 2177–2194, doi:10.1175/1520-0442(2000)013<2177:IBTAVA>2.0.CO;2.

Schneider, U., A. Becker, P. Finger, A. Meyer-Christoffer, B. Rudolf, M. Bruno, and M. Ziese, 2011: GPCC full data reanalysis, version 6.0 at 1.0°: Monthly land-surface precipitation from rain-gauges built on GTS-based and historic data. Global Precipitation Climatology Centre, doi:10.5676/DWD_GPCC/FD_M_V6_100.

Seager, R., N. Naik, W. Baethgen, A. Robertson, Y. Kushnir, J. Nakamura, and S. Jurburg, 2010: Tropical oceanic causes of interannual to multidecadal precipitation variability in southeast South America over the past century. *J. Climate*, **23**, 5517–5539, doi:10.1175/2010JCLI3578.1.

Silva, G. A., T. Ambrizzi, and J. A. Marengo, 2009: Observational evidences on the modulation of the South American low level jet east of the Andes according the ENSO variability. *Ann. Geophys.*, **27**, 645–657, doi:10.5194/angeo-27-645-2009.

Silva, V. B. S., and V. E. Kousky, 2012: The South American monsoon system: Climatology and variability. *Modern Climatology*, S.-Y. Wang, Ed., InTech, 123–152, doi:10.5772/38565.

Silvestri, G. E., 2004: El Niño signal variability in the precipitation over southeastern South America during the austral summer. *Geophys. Res. Lett.*, **31**, L18206, doi:10.1029/2004GL020590.

Smith, T. M., R. W. Reynolds, T. C. Peterson, and J. Lawrimore, 2008: Improvements to NOAA's historical merged land–ocean surface temperature analysis (1880–2006). *J. Climate*, **21**, 2283–2296, doi:10.1175/2007JCLI2100.1.

Stohl, A., and P. James, 2004: A Lagrangian analysis of the atmospheric branch of the global water cycle. Part I: Method description, validation, and demonstration for the August 2002 flooding in central Europe. *J. Hydrometeor.*, **5**, 656–678, doi:10.1175/1525-7541(2004)005<0656:ALAOTA>2.0.CO;2.

——, and ——, 2005: A Lagrangian analysis of the atmospheric branch of the global water cycle. Part II: Earth's river catchments, ocean basins, and moisture transports between them. *J. Hydrometeor.*, **6**, 961–984, doi:10.1175/JHM470.1.

——, C. Forster, A. Frank, P. Seibert, and G. Wotawa, 2005: Technical note: The Lagrangian particle dispersion model FLEXPART version 6.2. *Atmos. Chem. Phys.*, **5**, 2461–2474, doi:10.5194/acp-5-2461-2005.

Trenberth, K. E., 1997: The definition of El Niño. *Bull. Amer. Meteor. Soc.*, **78**, 2771–2777, doi:10.1175/1520-0477(1997)078<2771:TDOENO>2.0.CO;2.

Tsonis, A. A., K. Swanson, and S. Kravtsov, 2007: A new dynamical mechanism for major climate shifts. *Geophys. Res. Lett.*, **34**, L13705, doi:10.1029/2007GL030288.

Vera, C., G. Silvestri, V. Barros, and A. Carril, 2004: Differences in El Niño response over the Southern Hemisphere. *J. Climate*, **17**, 1741–1753, doi:10.1175/1520-0442(2004)017<1741:DIENRO>2.0.CO;2.

Wang, X., and C. Wang, 2014: Different impacts of various El Niño events on the Indian Ocean dipole. *Climate Dyn.*, **42**, 991–1005, doi:10.1007/s00382-013-1711-2.

Wu, R., and B. P. Kirtman, 2004: Understanding the impacts of the Indian Ocean on ENSO variability in a coupled GCM. *J. Climate*, **17**, 4019–4031, doi:10.1175/1520-0442(2004)017<4019:UTIOTI>2.0.CO;2.

Xue, Y., T. M. Smith, and R. W. Reynolds, 2003: Interdecadal changes of 30-yr SST normal during 1871–2000. *J. Climate*, **16**, 1601–1612, doi:10.1175/1520-0442-16.10.1601.

Yoo, G. H., J. S. Kug, J. Y. Park, and F. F. Jin, 2013: Sea surface temperature in the north tropical Atlantic as a trigger for El Niño/Southern Oscillation events. *Nat. Geosci.*, **6**, 112–116, doi:10.1038/ngeo1686.

Zebiak, S. E., 1993: Air–sea interaction in the equatorial Atlantic region. *J. Climate*, **6**, 1567–1586, doi:10.1175/1520-0442(1993)006<1567:AIITEA>2.0.CO;2.

Zemp, D. C., C. F. Schleussner, H. M. J. Barbosa, R. J. Van der Ent, J. F. Donges, J. Heinke, G. Sampaio, and A. Rammig, 2014: On the importance of cascading moisture recycling in South America. *Atmos. Chem. Phys.*, **14**, 13 337–13 359, doi:10.5194/acp-14-13337-2014.